NACA RM E55I09

NACA

RESEARCH MEMORANDUM

EFFECT OF INLET-AIR-FLOW DISTORTIONS ON STEADY-STATE PERFORMANCE OF J65-B-3 TURBOJET ENGINE

By Ivan D. Smith, W. M. Braithwaite, and Howard F. Calvert

Lewis Flight Propulsion Laboratory
Cleveland, Ohio

NATIONAL ADVISORY COMMITTEE
FOR AERONAUTICS

WASHINGTON
January 25, 1956
Declassified July 28, 1960

NATIONAL ADVISORY COMMITTEE FOR AERONAUTICS

RESEARCH MEMORANDUM

EFFECT OF INLET-AIR-FLOW DISTORTIONS ON STEADY-STATE PERFORMANCE OF J65-B-3 TURBOJET ENGINE

By Ivan D. Smith, W. M. Braithwaite, and Howard F. Calvert

SUMMARY

The effects of inlet-air-flow distortions on the performance of the J65-B-3 turbojet engine were determined in an altitude test chamber over a range of altitudes from 15,000 to 50,000 feet at a flight Mach number of 0.8. The configurations investigated included two radial distortions having different passage penetration and one circumferential distortion. All distortions investigated had approximately a 20-percent total-pressure variation at rated corrected engine speed.

The radial inlet-air-flow distortions "washed out" in the first few compressor stages and, therefore, affected only the compressor performance. The circumferential inlet-air-flow distortion carried completely through the engine and had a small effect on component efficiencies. For rated exhaust-gas temperatures and fixed-area exhaust-nozzle operation, the net-thrust loss caused by the effect of radial distortion on compressor efficiency and air flow was about 4 percent, while the net-thrust loss caused by the effect of circumferential distortion on the turbine temperature profile was 3 percent at an altitude of 35,000 feet.

INTRODUCTION

Inlet pressure or air-flow distortions of appreciable magnitude at the inlet of turbojet engines have been encountered in flight with many current aircraft. These distortions result from internal-flow separation within the diffuser or operation at off-design inlet conditions. As shown by previous investigations (refs. 1 to 3), inlet-air-flow distortions may result in reductions in thrust, high local turbine temperatures, compressor stall, compressor blade vibration, decreased acceleration rates, and combustor blow-out.

The effects of inlet-air-flow distortions on the performance of the J65-B-3 turbojet engine were determined in an NACA Lewis altitude test chamber as part of an evaluation of inlet-air-flow distortions on a

number of current turbojet engines. Inlet-air-flow distortions investigated included two radial distortions having different passage penetration and one circumferential distortion. The three distortions had approximately a 20-percent inlet-total-pressure variation at rated corrected engine speed.

Data taken over a range of altitudes from 15,000 to 50,000 feet at a flight Mach number of 0.8 are presented to show the effect of inlet-air-flow distortions on component performance, over-all engine pumping characteristics, net thrust, and specific fuel consumption. The effect of inlet-air-flow distortions on the surge and acceleration characteristics of the J65-B-3 turbojet engine is presented in reference 1.

APPARATUS

Facility

The installation of the J65-B-3 turbojet engine in an altitude test chamber is shown in figure 1. Dry air was supplied to the engine inlet at the total pressure and temperature of the desired flight condition. The static pressure in the altitude test chamber was decreased to correspond to the desired altitude.

Engine

The J65-B-3 turbojet engine has a 13-stage axial-flow compressor, an annular prevaporizing-type combustion chamber, and a two-stage turbine. At military rated conditions, the engine speed is 8300 rpm and the turbine-outlet temperature is 1166° F. The engine was equipped with a fixed-area exhaust nozzle sized to give rated turbine-outlet temperature at rated engine speed during static sea-level operation. Clamshell-type flaps were installed on the exhaust nozzle to allow data to be taken with exhaust-nozzle areas smaller than rated.

Air was bled from the fifth stage of the compressor for oil-mist lubrication and discharged overboard. The overboard air flow, which is composed of oil-mist bleed air and compressor-discharge seal leakage, amounted to about 1.5 percent of the engine-inlet air flow. The turbine shroud was cooled by air bled from the combustor (approximately 1.75 percent), the bleed air returning to the mainstream downstream of the turbine.

The fuel used throughout this investigation was MIL-F-5624A, grade JP-4, with a hydrogen-carbon ratio of 0.169 and a lower heating value of 18,700 Btu per pound.

Distortion Screens

Screens used to introduce inlet-air-flow distortions were located 39 inches ahead of the inlet guide vanes. A 4×4 mesh backing screen, to which blockage screens were attached, covered the entire passage (fig. 2). Two radial distortion screens having different passage penetration (figs. 2(b) and (c)) blocked the annulus next to the outer wall of the passage. A cylindrical sheet-metal splitter duct starting at the inner edge of the blockage screen and extending to the inlet guide vanes was installed with both radial distortions. The blocked (low-pressure) passages covered approximately 30 and 50 percent of the passage depth at the inlet guide vanes. Hereinafter the radial distortions will be referred to as a 30-percent- and a 50-percent-penetration distortion. One circumferential distortion-screen assembly (fig. 2(d)) with blockage varying at 45° intervals around the passage was used to introduce an inlet-air-flow distortion having a gradual variation from maximum to minimum around the passage.

Instrumentation

Instrumentation at various stations throughout the engine are shown in figure 3. All pressures were measured with manometers and recorded photographically. Temperatures were measured with either iron-constantan or chromel-alumel thermocouples and recorded by a self-balancing potentiometer. Fuel flow was measured by calibrated rotometers. Compressor rotating-stall zones were determined with hot-wire anemometers, installed in the stator passages of the first three stages, in conjunction with an oscilloscope.

PROCEDURE

All data were taken at a flight Mach number of 0.8 at the following altitudes:

Distortion	Altitude, ft			
	Rated exhaust-nozzle area			Variable exhaust-nozzle area
	15,000	35,000	50,000	35,000
Uniform flow	x	x	x	x
Radial, 30-percent penetration	x	x	x	x
Radial, 50-percent penetration		x		
Circumferential		x		x

The inlet total pressure of the desired flight condition was set in the unblocked section of the duct downstream of the distortion screen. Data were taken over a range of corrected engine speeds from 5000 to 9000 rpm with rated exhaust-nozzle area and from 5000 to 7000 rpm with variable exhaust-nozzle area in approximately 500 rpm increments. Variable-exhaust-nozzle-area data were obtained between the rated-exhaust-nozzle-area operating line and the turbine temperature limit primarily to map out the rotating-stall region. The operating limit of the engine was represented by either a turbine-outlet temperature of 1166° F or a mechanical engine speed of 8300 rpm.

Definitions of symbols and methods of calculation are presented in the appendixes.

RESULTS AND DISCUSSION

Pressure and Temperature Profiles

Engine-inlet total-pressure variation, which is a function of the engine air flow, is shown in figure 4 for a range of corrected engine speeds from 5000 to 9000 rpm for all three distortions. At rated corrected engine speed (8300 rpm) both radial distortions had approximately 21 percent total-pressure variation and the circumferential distortion had approximately 19 percent total-pressure variation.

Pressure and temperature profiles (figs. 5 to 8) are shown for a corrected engine speed of 8300 rpm at the following engine locations.

Engine location	Radial distortions		Circumferential distortion	
	Pressure	Temperature	Pressure	Temperature
Compressor inlet	x		x	
Compressor 2nd stage	x	x		
Compressor 4th stage	x	x		
Compressor outlet	x	x	x	x
Turbine outlet	x	x	x	x

The compressor-inlet pressure profiles were measured in an inlet-guide-vane passage with the radial distortions and at station 2 with the circumferential distortion. The circumferential compressor-inlet total-pressure profile was assumed to be symmetrical on both halves of the

passage, and consequently only one-half of the inlet circumference was instrumented. Although the profiles shown are for an altitude of 35,000 feet and a flight Mach number of 0.8, they should also apply to other flight conditions.

As shown by the data of figure 5, radial pressure profiles were essentially "washed out" in the first four compressor stages. Increased pressure ratio at the blade tips (combination of figs. 5(a) and (b)) produced a high local temperature at the blade tips (fig. 6) which persisted throughout the compressor but was negligible at the outlet of the turbine. Circumferential pressure profiles carried throughout the engine but decreased in magnitude (fig. 7), resulting in approximately a 3-percent average variation in both pressure and temperature at the outlet of the turbine (figs. 7 and 8).

Component Performance

Efficiencies. - As shown by the data of figure 5, the radial distortions affect primarily the inlet stages of the compressor. In these stages the section of each blade in the blocked (low inlet pressure) portion of the annulus will have a lower axial inlet velocity and, therefore, will be operating at a higher angle of attack than normal. At low engine speeds the inlet stages of the compressor are normally operating at high angles of attack and generally in a stalled condition and, therefore, the effect of radial inlet-air-flow distortions on compressor performance at low speeds is more severe than at high speeds (fig. 9), even though the distortions are smaller. This decrease in performance of the inlet stages of the compressor at low engine speeds with a radial inlet-air-flow distortion can be seen more clearly in figure 10, which presents the characteristic curves for compressor stages 1 and 2, and 3 and 4. Also, the radial inlet-air-flow distortions decreased the peak pressure coefficient of the first two stages and caused rotating stall to persist to higher engine speeds.

The decrease in compressor efficiency at low engine speeds caused by the radial inlet-air-flow distortion was 1 and 4 percent at altitudes of 15,000 and 50,000 feet, respectively (fig. 9). At corrected engine speeds between 7000 rpm and rated, radial distortions of the magnitude investigated had a negligible effect on compressor efficiency. At corrected engine speeds above rated, the radial inlet-air-flow distortions became large, resulting in a small decrease in compressor efficiency.

Compressor efficiency was essentially unaffected by a circumferential distortion of the magnitude investigated (fig. 9). With circumferential inlet-air-flow distortion the blocked and unblocked portions of the compressor are operating at the same corrected engine speed. The blocked portion will be operating at a higher pressure ratio than normal, and the

unblocked portion will be operating at a lower pressure ratio than normal, so that all portions will essentially shift their respective operating points along a constant-corrected-engine-speed line of the uniform-inlet-flow compressor map (ref. 2). In this case the shift in the operating points of all portions of the compressor was not sufficient to cause an appreciable change in the over-all compressor efficiency.

Within the range of accuracy, distortion had negligible effect on combustion and turbine efficiencies (figs. 11 and 12), which is similar to the results of references 2 and 3.

Compressor maps. - The compressor maps for uniform flow, 30-percent-penetration radial distortion, and circumferential distortion are shown in figures 13(a), (b), and (c), respectively, for an altitude of 35,000 feet and a flight Mach number of 0.8. An attempt has been made to show the regions where different numbers of rotating stalls exist, even though the boundaries between the regions are not well defined. A three-rotating-stall-zone pattern seemed to be the most stable, with or without distortion; and a peak in compressor pressure ratio, at a given corrected engine speed, generally occurred within this region. A stable two-zone-rotating-stall pattern rarely occurred, and frequently operation went directly between a three- and a one-zone-rotating-stall pattern. The formation of one-zone rotating stall is called the steady-state stall limit, even though a complete stall does not exist because at this point the compressor efficiency and, therefore, the pressure ratio and the air flow decreased markedly, and the turbine generally encountered overtemperature in this region.

The circumferential distortion (fig. 13(c)) had a negligible effect on the rotating-stall characteristics and the stall limit. The 30-percent-penetration radial distortion (fig. 13(b)) decreased the stall limit at intermediate engine speeds (6000 to 6500 rpm); caused a widening of the rotating-stall regions at engine speeds below 6000 rpm, so that the rated-exhaust-nozzle operating line passed through the region of four-zone rotating stall instead of five zone; and caused rotating stall to persist to higher engine speeds. Radial distortion also decreased the air flow at a given corrected engine speed. Generally, the effects and trends obtained from these distortions are characteristic of those obtained from similar distortions investigated on other engines.

Steady-state and transient limits. - In the rotating-stall region a higher compressor pressure ratio can be obtained by transient operation than by steady-state operation. As discussed previously, the lines of constant corrected engine speed in the rotating-stall region of the compressor map reach a peak in, or near, the three-rotating-stall-zone region. These peaks represent the maximum compressor pressure ratios that can be obtained by steady-state operation.

Data in reference 1 indicate that, during a fuel-step acceleration of this engine, complete compressor stall, frequently accompanied by surge, occurs. In the rotating-stall region the compressor pressure ratio just prior to complete stall was higher than the maximum compressor pressure ratio (not the pressure ratio at the stall limit) obtainable during steady-state operation at the same corrected engine speed. These two compressor-pressure-ratio limits are shown in relation to the rated-exhaust-nozzle operating line in figure 14 for uniform inlet flow. Insufficient instrumentation prevented determination of the exact phenomenon which allowed the transient compressor pressure ratio to exceed the steady-state maximum value. However, the data of reference 4 show that even during the small fuel steps reported therein all the rotating-stall patterns formed in the normal steady-state sequence do not have time to form. At speeds above the rotating-stall region the steady-state limit was a turbine temperature limit, which is also shown in figure 14.

The effect of inlet-air-flow distortions on the maximum steady-state compressor pressure ratios, steady-state temperature limits, transient stall limits, and rated-exhaust-nozzle operating lines is shown in figure 15. In the rotating-stall region, the radial inlet-air-flow distortions decreased both the steady-state and the transient compressor-pressure-ratio limits more than the circumferential distortion did. The radial distortions extended the rotating-stall region to a higher engine speed, as previously indicated, which caused a considerable decrease in the maximum compressor pressure ratios in the range of corrected engine speeds from 6200 to 6800 rpm. The steady-state operating pressure ratios decreased slightly with both radial distortions, whereas the pressure ratios for the circumferential distortion were the same as for uniform inlet flow.

Over-All Engine Performance

Pumping characteristics. - The engine pumping characteristics are presented in figures 16(a), (b), and (c) at a flight Mach number of 0.8 and altitudes of 15,000, 35,000, and 50,000 feet, respectively. The pumping characteristics plotted are engine total-temperature ratio, engine total-pressure ratio, corrected engine air flow, and corrected fuel flow.

In general, the distortions, both circumferential and radial, did not affect the engine pumping characteristics more than 1 to 2 percent in the high-speed range except that the radial distortions reduced the corrected air flow as much as 3 to 4 percent. The variations in pressure and temperature ratio reflect the changes in component efficiencies already discussed.

Net thrust and specific fuel consumption. - Associated with the losses in engine pumping characteristics due to inlet-air-flow distortions are a reduction in net thrust and possibly an increase in specific fuel consumption. For the engine operating with a fixed-area exhaust nozzle and at rated exhaust-gas temperature, the loss in thrust resulting from both radial distortions investigated amounted to about 4 percent for an altitude of 35,000 feet and flight Mach number of 0.8. This loss in thrust results from a decrease in compressor efficiency of about 1 percent and a loss in air flow of 3 percent. Accompanying the thrust loss was an increase in specific fuel consumption of about 2 percent.

With the circumferential distortion there was no measurable thrust loss due to a decrease in component efficiencies. However, there is a thrust loss because of the turbine gas-temperature profile (fig. 8), which requires a reduction in engine speed to prevent local turbine temperatures from exceeding the limit. The turbine-outlet temperature profile in figure 8 is at rated corrected engine speed and not rated turbine-outlet temperature, but the profile at rated turbine-outlet temperature is almost identical. For a circumferential distortion of the magnitude investigated, a 2-percent reduction in average exhaust-gas temperature was required. This was obtained by a 1.3-percent reduction in corrected engine speed and resulted in approximately a 3-percent loss in net thrust. Figure 17 presents the net-thrust loss that would be associated with any reduction in average exhaust-gas temperature between 0 and 10 percent for an altitude of 35,000 feet and flight Mach number of 0.8.

The loss in net thrust resulting from the turbine gas-temperature profile did not cause the specific fuel consumption to increase but actually to decreases slightly (about 1 percent), because the reduction in engine speed shifted the compressor operating point to a region of higher efficiency.

SUMMARY OF RESULTS

The following results were obtained from a determination of the effects of inlet-air-flow distortion on the J65-B-3 turbojet engine:

Two radial inlet-air distortions, both having total-pressure variations of 21 percent at rated corrected engine speed, "washed-out" in the first few compressor stages. Because these radial distortions did not persist throughout the engine, combustor and turbine performance was unaffected. The radial distortions affected the rotating stall of the compressor, causing the steady-state stall limit at intermediate engine speeds to decrease, and extended the entire rotating-stall region to higher engine speeds. The decrease in air flow and the slight decrease in compressor efficiency caused by the radial distortions decreased the rated net thrust approximately 4 percent.

An approximately sinusoidal circumferential inlet-air distortion, having a total-pressure variation of 19 percent at rated corrected engine speed, carried completely through the engine but decreased in magnitude in passing through the engine. This distortion had a small effect on component efficiencies. The resulting distortion at the turbine caused local turbine-outlet temperatures to exceed the temperature limit. The decrease in engine speed necessary to prevent the turbine from encountering overtemperature resulted in a decrease in rated net thrust of approximately 3 percent at an altitude of 35,000 feet and flight Mach number of 0.8.

Lewis Flight Propulsion Laboratory
National Advisory Committee for Aeronautics
Cleveland, Ohio, September 13, 1955

APPENDIX A

SYMBOLS

The following symbols are used in this report:

A	area, sq ft
C	coefficient
D	diameter, ft
F	thrust, lb
g	acceleration due to gravity, 32.2 ft/sec^2
H	enthalpy, Btu/lb
K	constant
M	Mach number
N	engine speed, rpm
P	total pressure, lb/sq ft abs
p	static pressure, lb/sq ft abs
R	gas constant, 53.3 ft-lb/(lb)($^\circ$R)
S	number of stages
T	total temperature, $^\circ$R
t	static temperature, $^\circ$R
V	velocity, ft/sec
w	flow rate, lb/sec or lb/hr
γ	ratio of specific heats
δ	ratio of total pressure to NACA standard sea-level static pressure
η	efficiency

θ ratio of total temperature to NACA standard sea-level static temperature

φ flow coefficient

ψ pressure coefficient

Subscripts:

a air

av average

b combustor

c compressor

D distorted

d discharge

F thrust

f fuel

g gas

j jet

m mean

max maximum

min minimum

n net

o overboard

s turbine shroud

t turbine

U uniform flow

0 free stream

1	inlet duct $29\frac{7}{8}$ in. upstream of distortion screens
2	inlet duct $19\frac{3}{8}$ in. downstream of distortion screens and $19\frac{5}{8}$ in. ahead of compressor-inlet guide vanes
3	compressor outlet
4	turbine inlet
5	turbine outlet
9	exhaust-nozzle inlet
10	exhaust-nozzle throat

APPENDIX B

METHODS OF CALCULATION

Average Pressures and Temperatures

The inlet total pressure P_1 was taken as the arithmetic average of 12 probes (two probes located 180° apart in each of six equal concentric areas).

The inlet static pressure p_1 was taken as the arithmetic average of four wall static taps located 90° apart.

The inlet total temperature T_1 was taken as the arithmetic average of six thermocouples (two thermocouples located 180° apart in each of three equal concentric areas).

The inlet total pressure P_2 for uniform flow and for the radial distortions was taken as the arithmetic average of eight integrating rakes (four rakes located 90° apart in each duct).

The inlet total pressure P_2 for the circumferential distortion was taken as the arithmetic average of 20 probes located on 20 equal concentric areas (every fourth probe located on same rake; rakes at 27°, 90°, 207°, and 297° clockwise from top looking downstream).

The pressure and temperature for the second- and fourth-stage stator were taken as the arithmetic average of five probes located on one rake and in five equal concentric areas.

The compressor-outlet total pressure P_3 was taken as the arithmetic average of 12 probes (three probes located at 70°, 188°, and 334° clockwise from top looking downstream in each of four equal concentric areas).

The compressor-outlet total temperature T_3 was taken as the arithmetic average of 12 probes (six on each of two rakes located 180° apart).

The turbine-inlet total pressure P_4 was calculated from P_3 and a curve of P_4/P_3 against $N/\sqrt{\theta_1}$ as determined experimentally in the program.

The turbine-outlet total pressure P_5 was taken as the arithmetic average of 15 probes (five probes on each of three rakes located at 99°, 213°, and 333° clockwise from top looking downstream).

The exhaust-nozzle-inlet total pressure P_9 was taken as the arithmetic average of 35 probes (five probes located 72° apart in each of seven equal concentric areas).

The exhaust-nozzle-inlet total temperature T_9 was taken as the arithmetic average of 30 thermocouples (five thermocouples located 72° apart in each of six equal concentric areas).

Air Flow

The engine-inlet air flow $w_{a,1}$ was calculated from one-dimensional compressible-flow relations (ref. 5) using the effective area and the average pressures and temperature at station 1. The effective area at station 1 was 4.754 square feet (A_1 = 4.851 sq ft, C_d = 0.98). Air bleeds and the addition of fuel resulted in the following mass flows at other stations:

$$w_{a,3} = w_{a,1} - w_{a,o}$$

$$w_{g,4} = w_{a,1} - w_{a,o} - w_{a,s} + w_f/3600$$

$$w_{g,9} = w_{a,1} - w_{a,o} + w_f/3600$$

Compressor Efficiency

The compressor efficiency is defined as the ratio of isentropic enthalpy rise to the actual enthalpy rise across the compressor. In terms of pressure and temperature, this becomes:

$$\eta_c = \frac{(P_3/P_2)^{\frac{\gamma_1-1}{\gamma_1}} - 1}{(T_3/T_1) - 1}$$

Combustion Efficiency

The combustion efficiency is defined as the ratio of actual enthalpy rise to the theoretical enthalpy rise across the engine:

$$\eta_b = \frac{\Delta H_a\Big]_1^9 + \frac{w_f}{3600 w_{a,1}} \left[\frac{A_m + B}{m + 1}\right]_{T_f}^{9} - \frac{w_{a,o}}{w_{a,1}} \Delta H_a\Big]_o^9}{\frac{w_f}{3600\ w_{a,1}}\ 18{,}700}$$

The term $\frac{A_m + B}{m + 1}$ is the difference between the enthalpy of carbon dioxide and water vapor in the burned mixture and the enthalpy of oxygen removed from the air by their formation (ref. 6).

Turbine Efficiency

The turbine efficiency is defined as the ratio of actual enthalpy drop to the isentropic enthalpy drop across the turbine. In terms of pressure and temperature, this becomes:

$$\eta_t = \frac{1 - \frac{T_9}{T_4}}{1 - \left(\frac{P_5}{P_4}\right)^{\frac{\gamma_4 - 1}{\gamma_4}}}$$

The turbine-inlet temperature T_4 was calculated by assuming that the turbine enthalpy drop equaled the compressor enthalpy rise:

$$H_{g,4} = \frac{w_{a,1}}{w_{g,4}} \Delta H_a\Big]_1^3 - \frac{w_{a,o}}{w_{g,4}} \Delta H_a\Big]_o^3 + H_{g,5}$$

The value of T_4 was then obtained from enthalpy tables.

Compressor Stage Performance

Pressure coefficient. - The pressure coefficient is defined by the following equation:

$$\psi = \frac{3600gR\gamma_1 T_1\left[\left(\frac{P_3}{P_2}\right)^{\frac{\gamma_1-1}{\gamma_1}} - 1\right]}{S(\pi D_m)^2(\gamma_1 - 1)N^2} = \frac{K_1 T_1}{N^2}\left[\left(\frac{P_3}{P_2}\right)^{\frac{\gamma_1-1}{\gamma_1}} - 1\right]$$

For stages 1 and 2, K_1 = 346,500; for stages 3 and 4, K_1 = 276,700.

Flow coefficient. - The flow coefficient is defined by the following equation (ref. 7):

$$\Phi = \frac{240Rw_{a,1}T_1}{\pi^2 D_m^3 P_2 N} = \frac{K_2 w_{a,1} T_1}{P_2 N}$$

For stages 1 and 2, K_2 = 143.7; for stages 3 and 4, K_2 = 174.8.

Net Thrust

Net thrust is defined by the following equation:

$$F_n = \frac{w_{g,10}}{g} V_{10} + (p_{10} - p_0)A_{10} - \frac{w_{a,1}}{g} V_0$$

For choked flow in the exhaust nozzle, it can be shown that (ref. 8)

$$\frac{w_{g,10}}{g} V_{10} + (p_{10} - p_0)A_{10} = C_{F_j} A_{10}\left[(\gamma_{10} + 1)\left(\frac{2}{\gamma_{10} + 1}\right)^{\frac{\gamma_{10}}{\gamma_{10}-1}} P_{10} - p_0\right]$$

From experimental data, C_{F_j} = 0.98 and A_{10} = 1.97 square feet.

$$f(\gamma_{10}) = (\gamma_{10} + 1)\left(\frac{2}{\gamma_{10} + 1}\right)^{\frac{\gamma_{10}}{\gamma_{10}-1}}$$

By assuming that $P_9 = P_{10}$, the net thrust then becomes:

$$F_n = 1.93\left[f(\gamma_{10})P_9 - p_0\right] - 1.525w_{a,1}M_0\sqrt{t_0}$$

REFERENCES

1. Fenn, David B., and Sivo, Joseph N.: Effect of Inlet Flow Distortion on Compressor Stall and Acceleration Characteristics of a J65-B-3 Turbojet Engine. NACA RM E55F20, 1955.

2. Walker, Curtis L., Sivo, Joseph N., and Jansen, Emmert T.: Effect of Unequal Air-Flow Distribution from Twin Inlet Ducts on Performance of an Axial-Flow Turbojet Engine. NACA RM E54E13, 1954.

3. Huntley, S. C., Sivo, Joseph N., and Walker, Curtis L.: Effect of Circumferential Total-Pressure Gradients Typical of Single-Inlet Duct Installations on Performance of an Axial-Flow Turbojet Engine. NACA RM E54K26a, 1955.

4. Calvert, Howard F., Braithwaite, Willis M., and Medeiros, Arthur A.: Rotating-Stall and Rotor-Blade-Vibration Survey of a 13-Stage Axial-Flow Compressor in a Turbojet Engine. NACA RM E54J18, 1955.

5. Turner, L. Richard, Addie, Albert N., and Zimmerman, Richard H.: Charts for the Analysis of One-Dimensional Steady Compressible Flow. NACA TN 1419, 1948.

6. Turner, L. Richard, and Bogart, Donald: Constant-Pressure Combustion Charts Including Effects of Diluent Addition. NACA Rep. 937, 1949. (Supersedes NACA TN's 1086 and 1655.)

7. Medeiros, Arthur A., Benser, William A., and Hatch, James E.: Analysis of Off-Design Performance of a 16-Stage Axial-Flow Compressor with Various Blade Modifications. NACA RM E52L03, 1953.

8. Sivo, Joseph N., and Fenn, David B.: A Method of Measuring Jet Thrust of Turbojet Engines in Flight Installations. NACA RM E53J15, 1954.

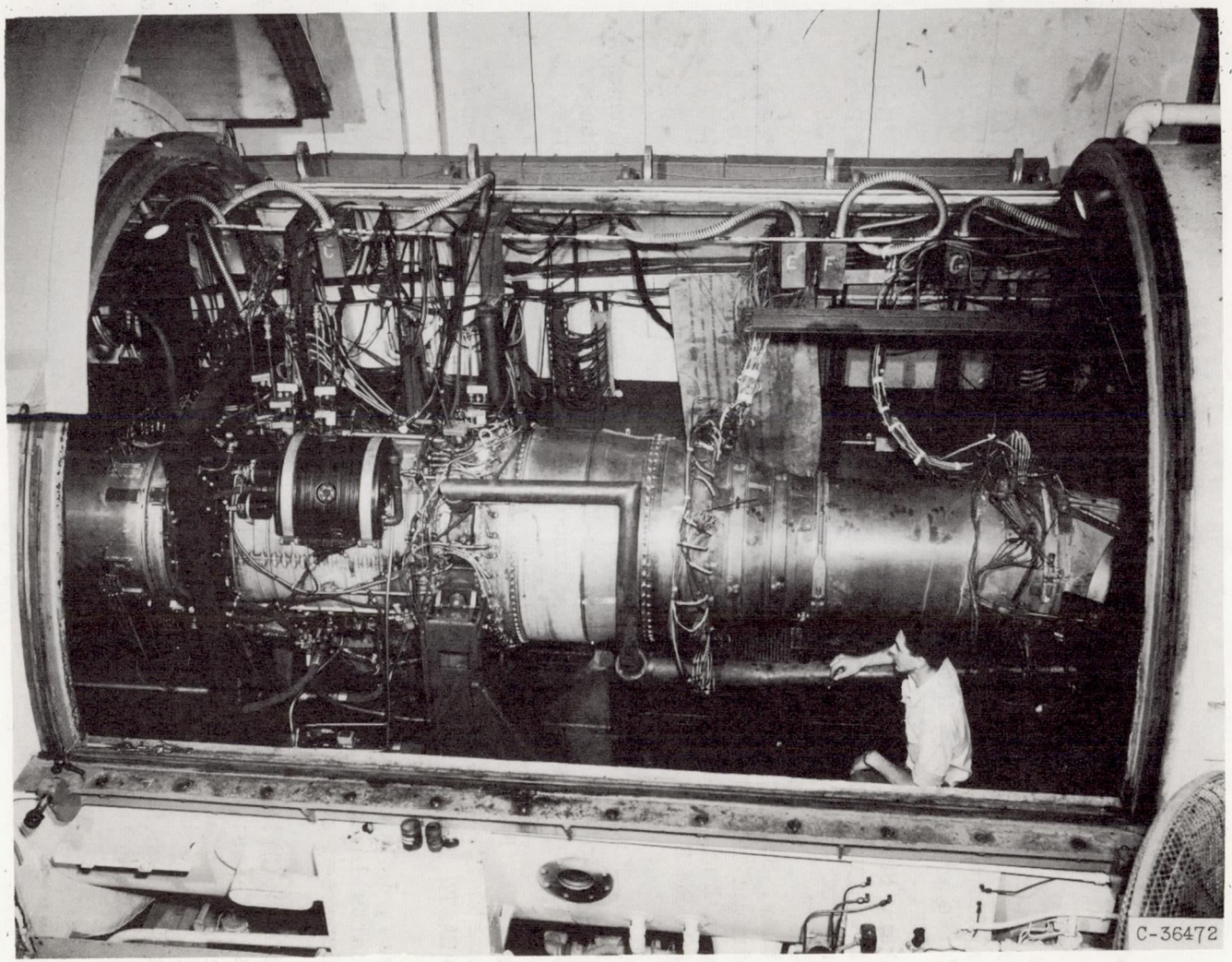

Figure 1. - Installation of J65-B-3 turbojet engine in altitude test chamber.

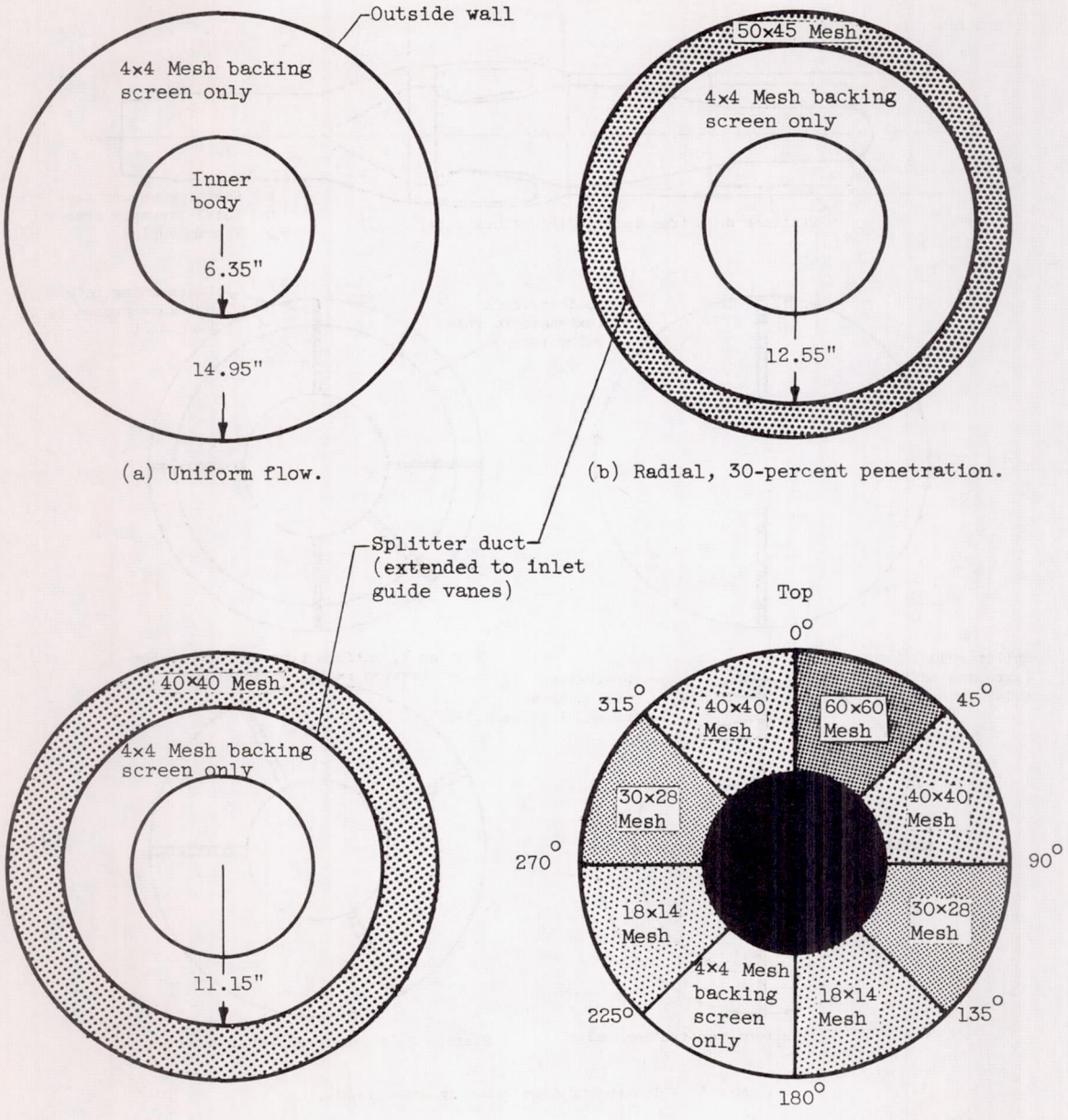

(a) Uniform flow.

(b) Radial, 30-percent penetration.

(c) Radial, 50-percent penetration.

(d) Circumferential.

Figure 2. - Screen locations for inlet-air distortions (looking downstream).

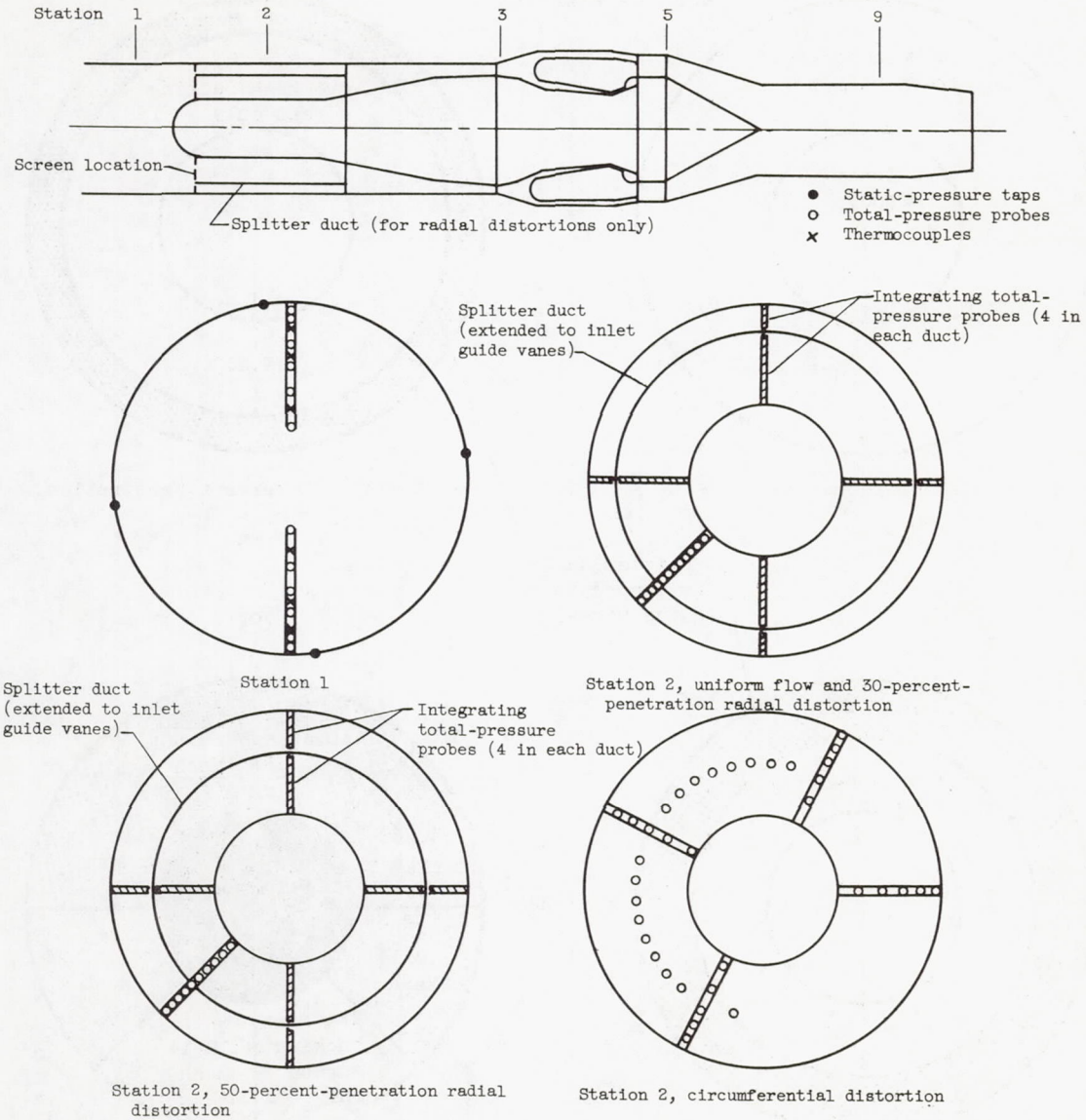

Figure 3. - Instrumentation (looking downstream).

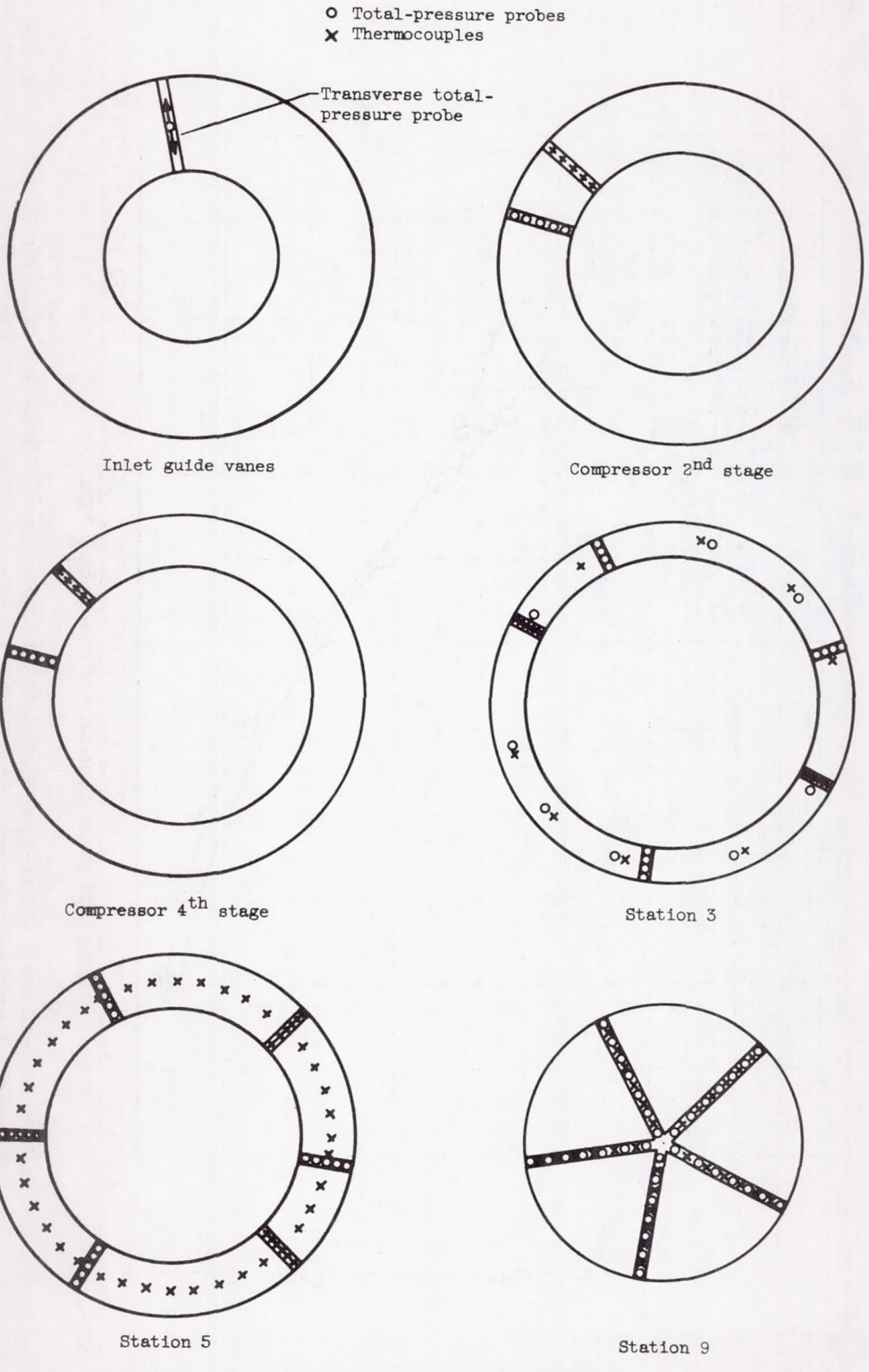

Figure 3. - Concluded. Instrumentation (looking downstream).

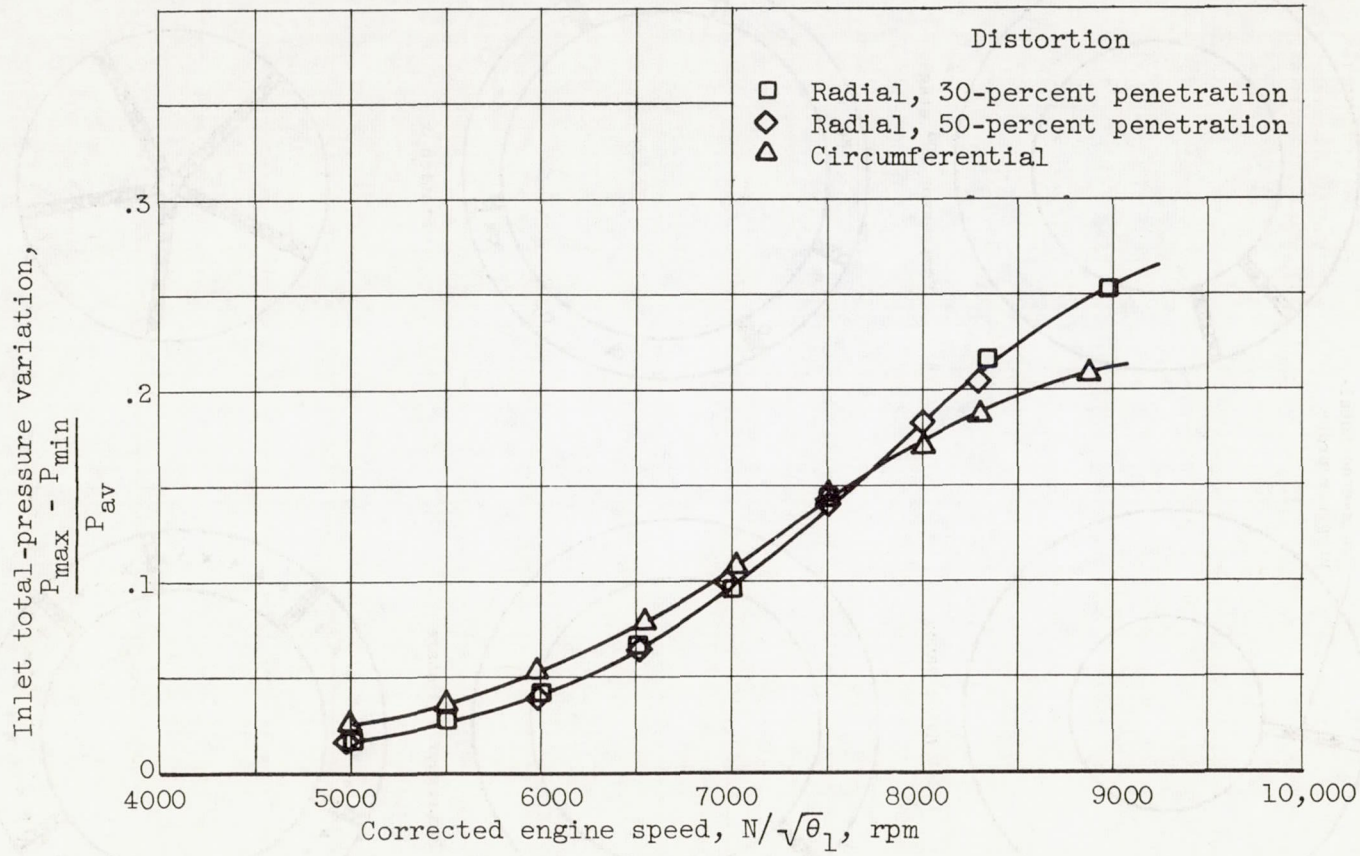

Figure 4. - Inlet total-pressure variation with distortion for a range of corrected engine speeds. Station 2.

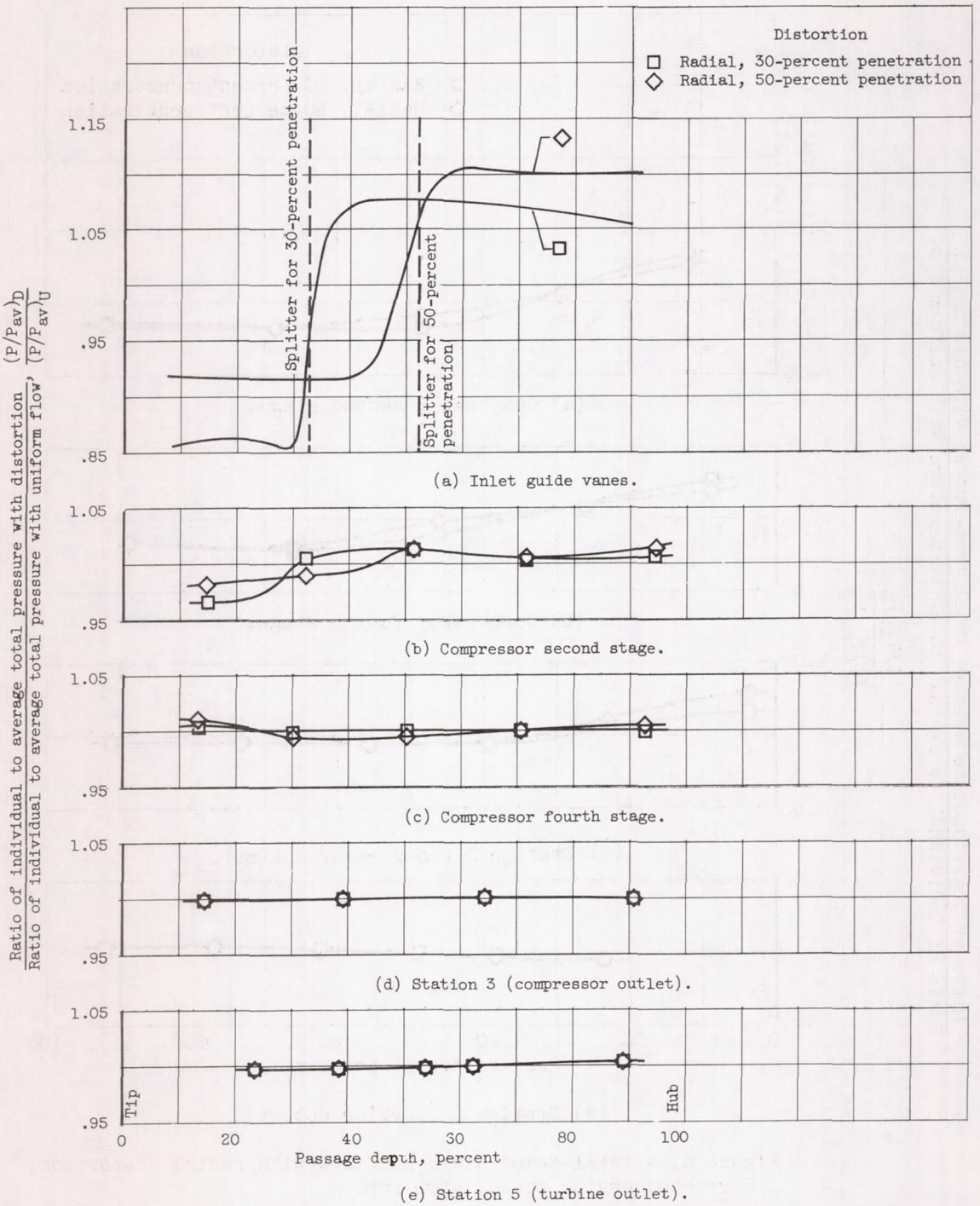

Figure 5. - Total-pressure profiles with radial distortion. Corrected engine speed, 8300 rpm.

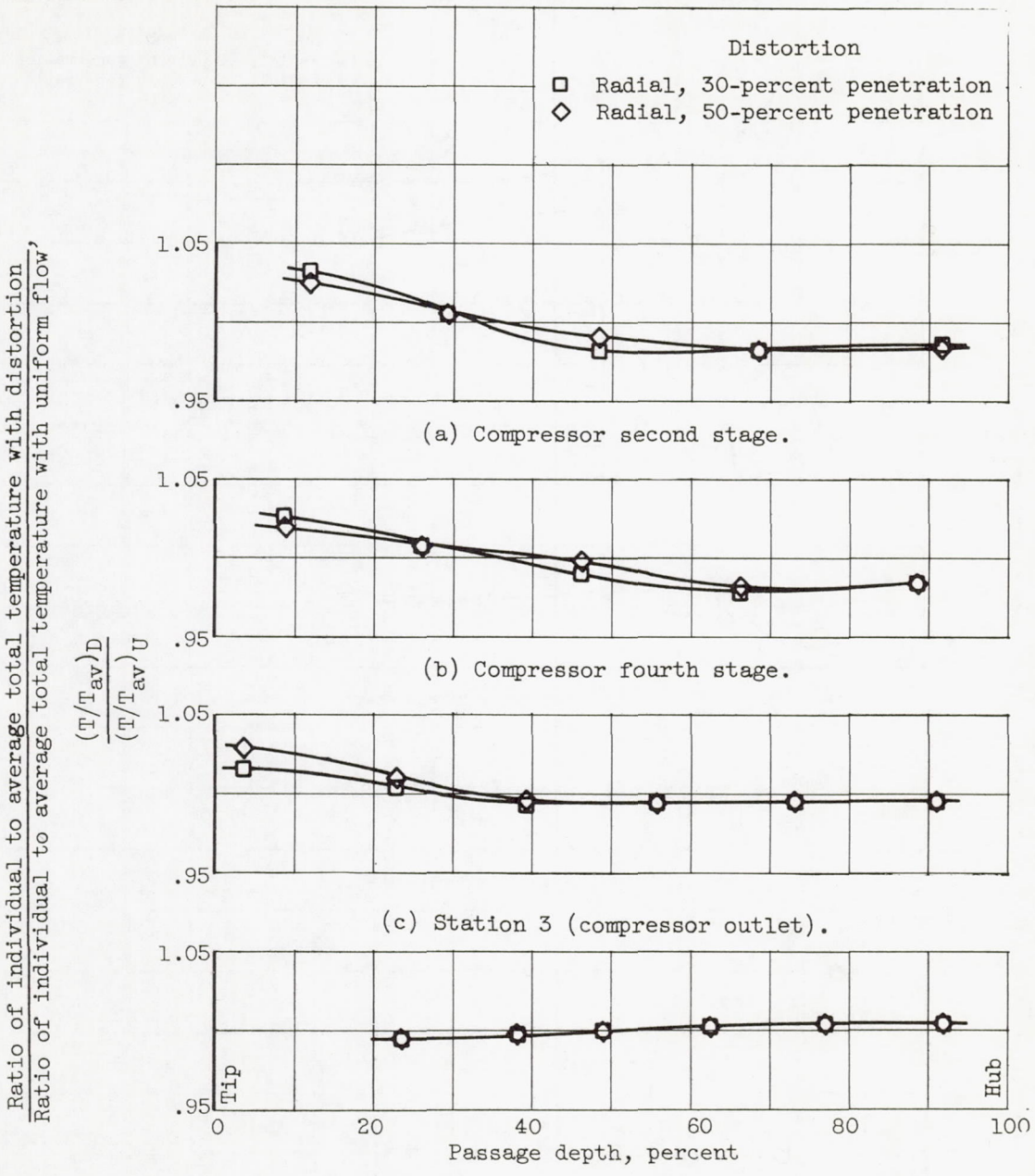

Figure 6. - Total-temperature profiles with radial distortion. Corrected engine speed, 8300 rpm.

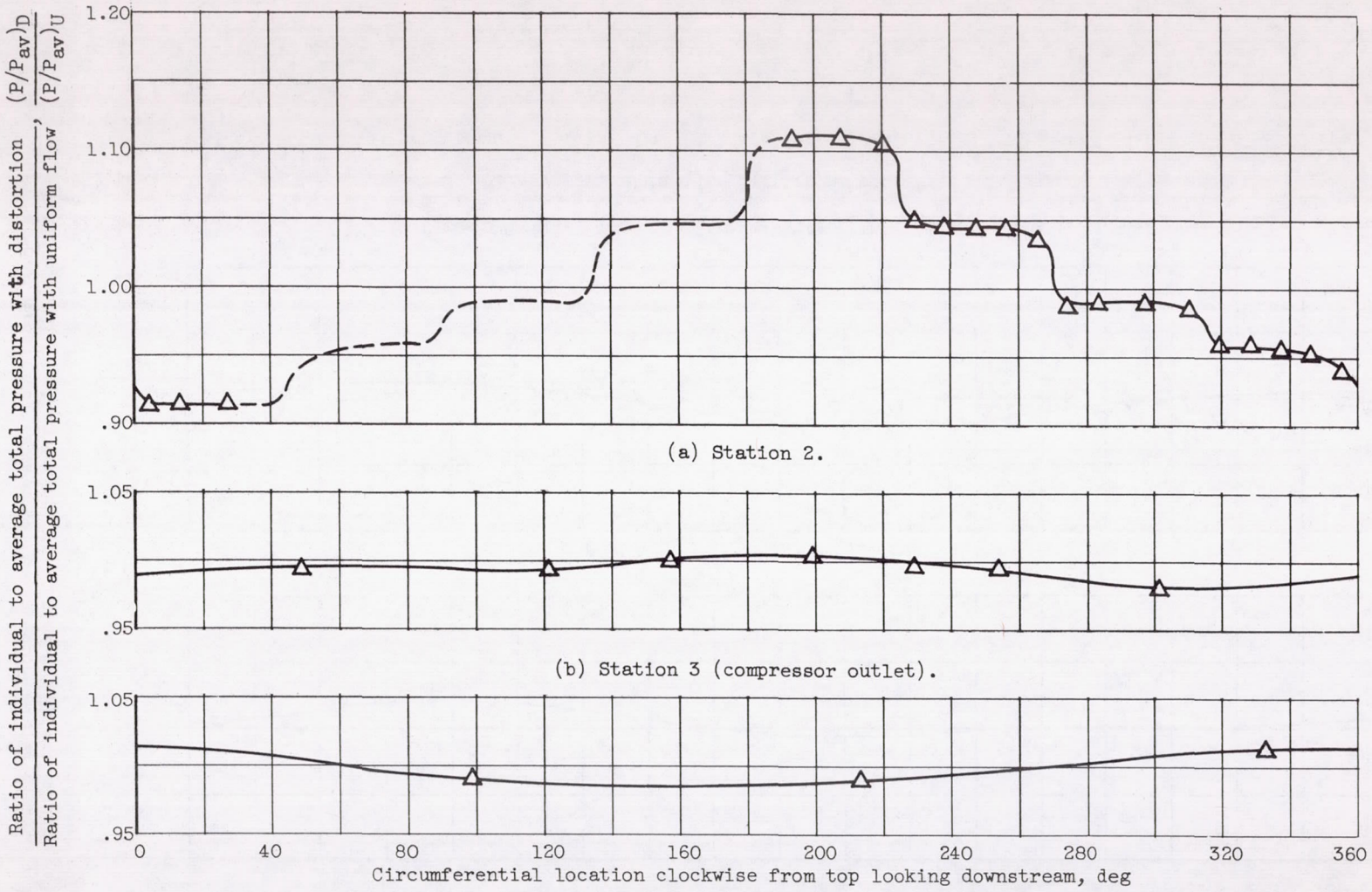

Figure 7. - Total-pressure profiles with circumferential distortion. Corrected engine speed, 8300 rpm.

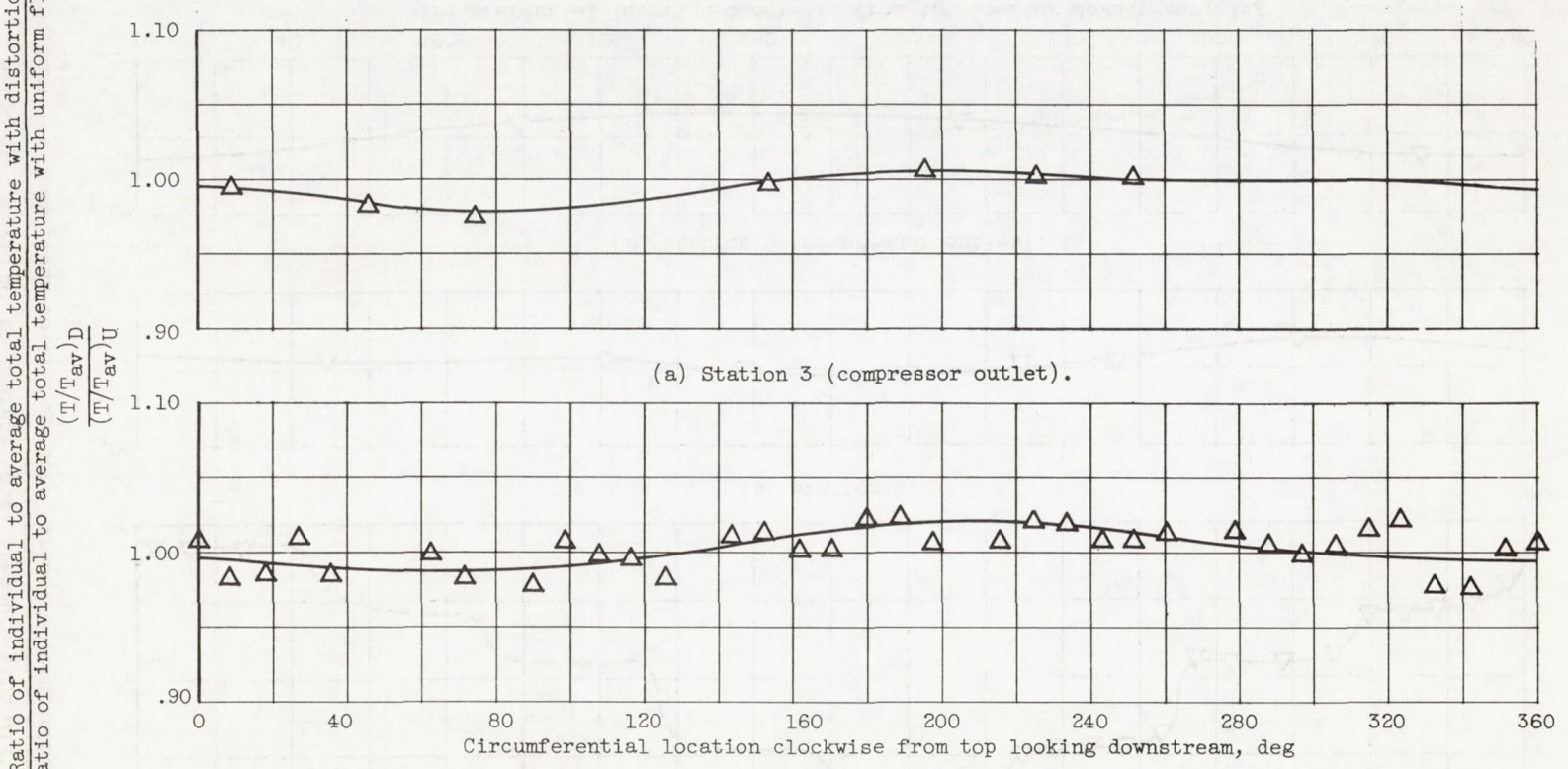

(a) Station 3 (compressor outlet).

(b) Station 5 (turbine outlet).

Figure 8. - Total-temperature profiles with circumferential distortion. Corrected engine speed, 8300 rpm.

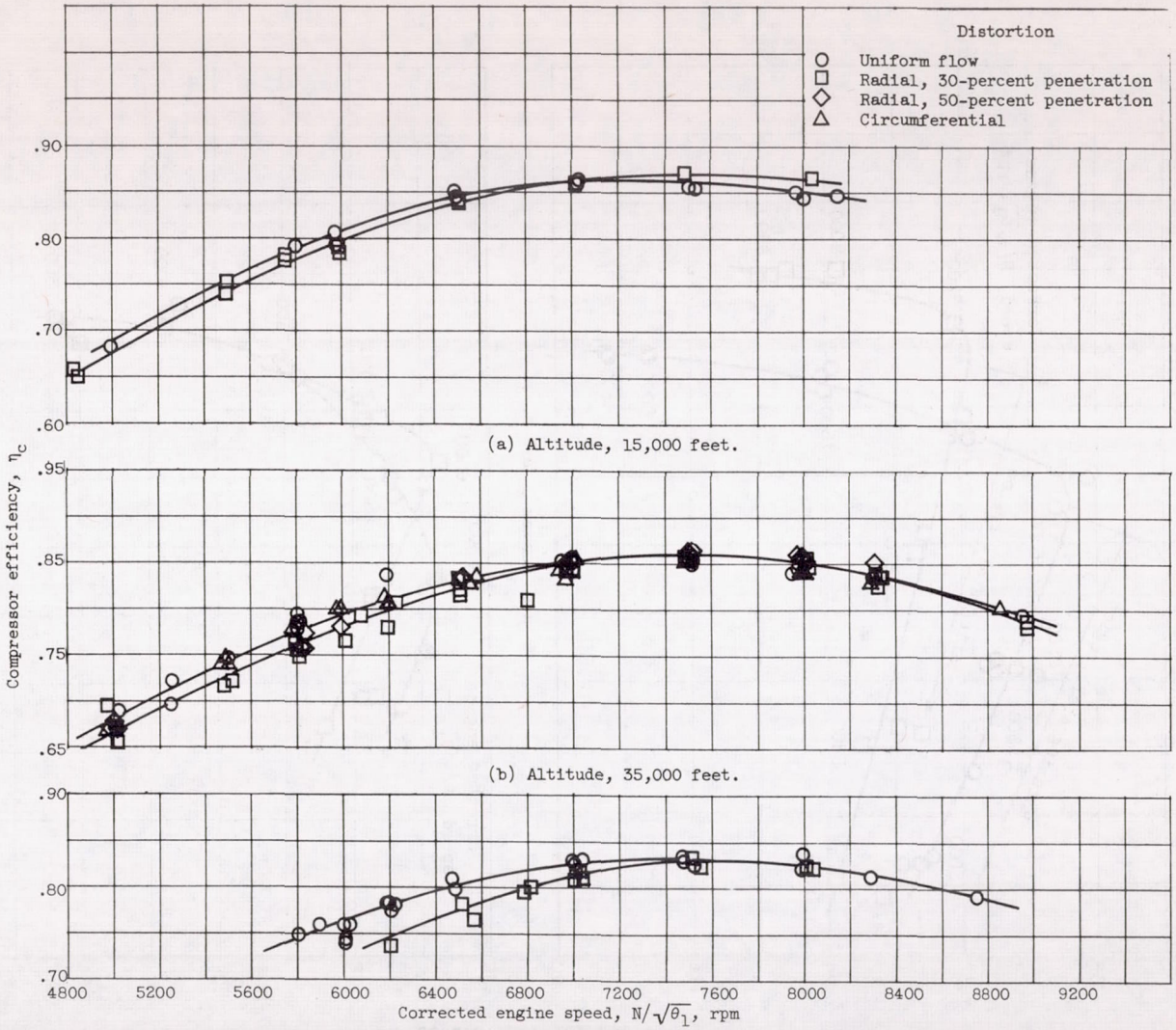

Figure 9. - Compressor efficiency with rated exhaust-nozzle area. Flight Mach number, 0.8.

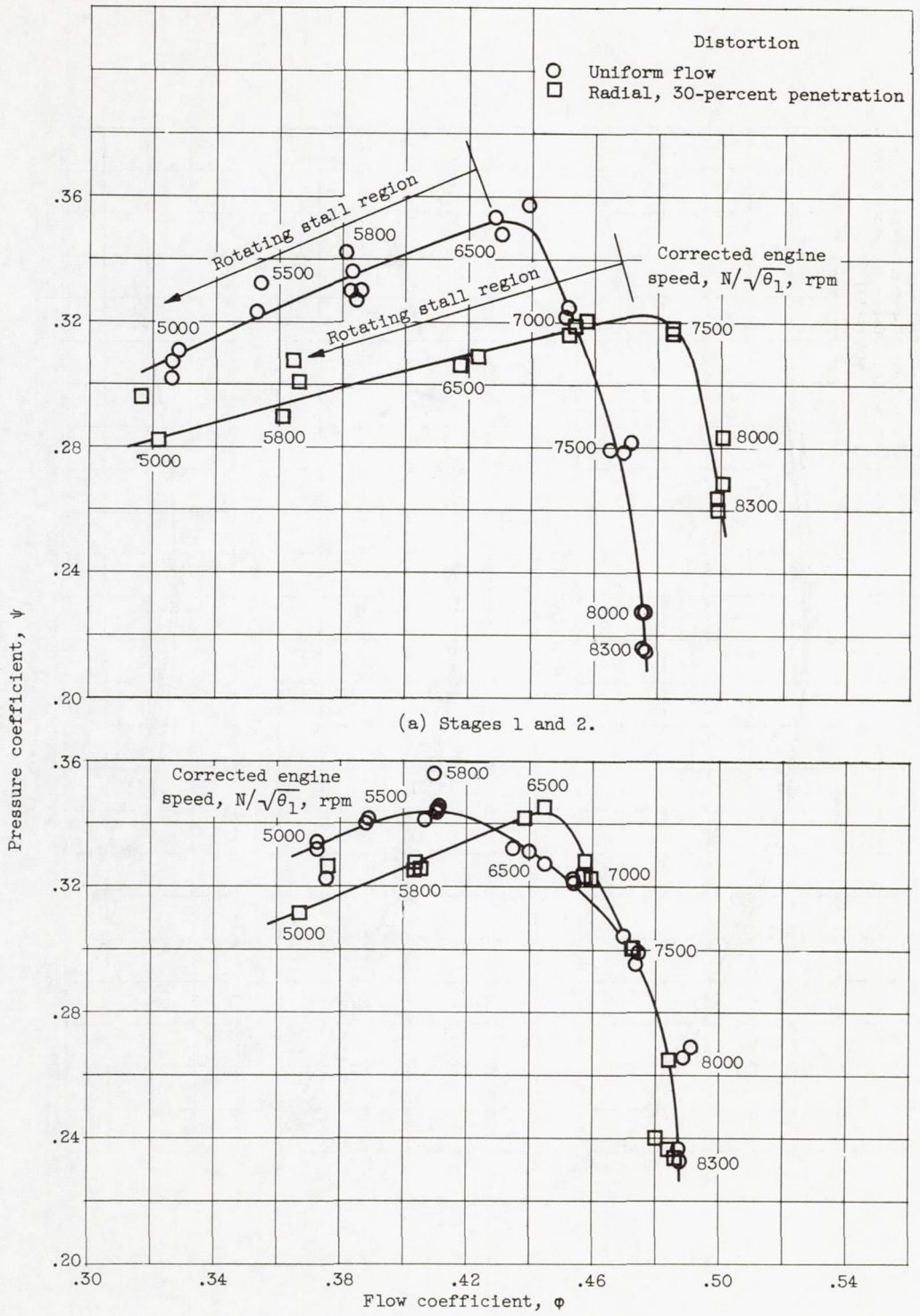

(a) Stages 1 and 2.

(b) Stages 3 and 4.

Figure 10. - Compressor-inlet-stage performance. Rated exhaust-nozzle area; altitude, 35,000 feet; flight Mach number, 0.8.

(a) Altitude, 15,000 feet.

(b) Altitude, 35,000 feet.

(c) Altitude, 50,000 feet.

Figure 11. - Combustion efficiency with rated exhaust-nozzle area. Flight Mach number, 0.8.

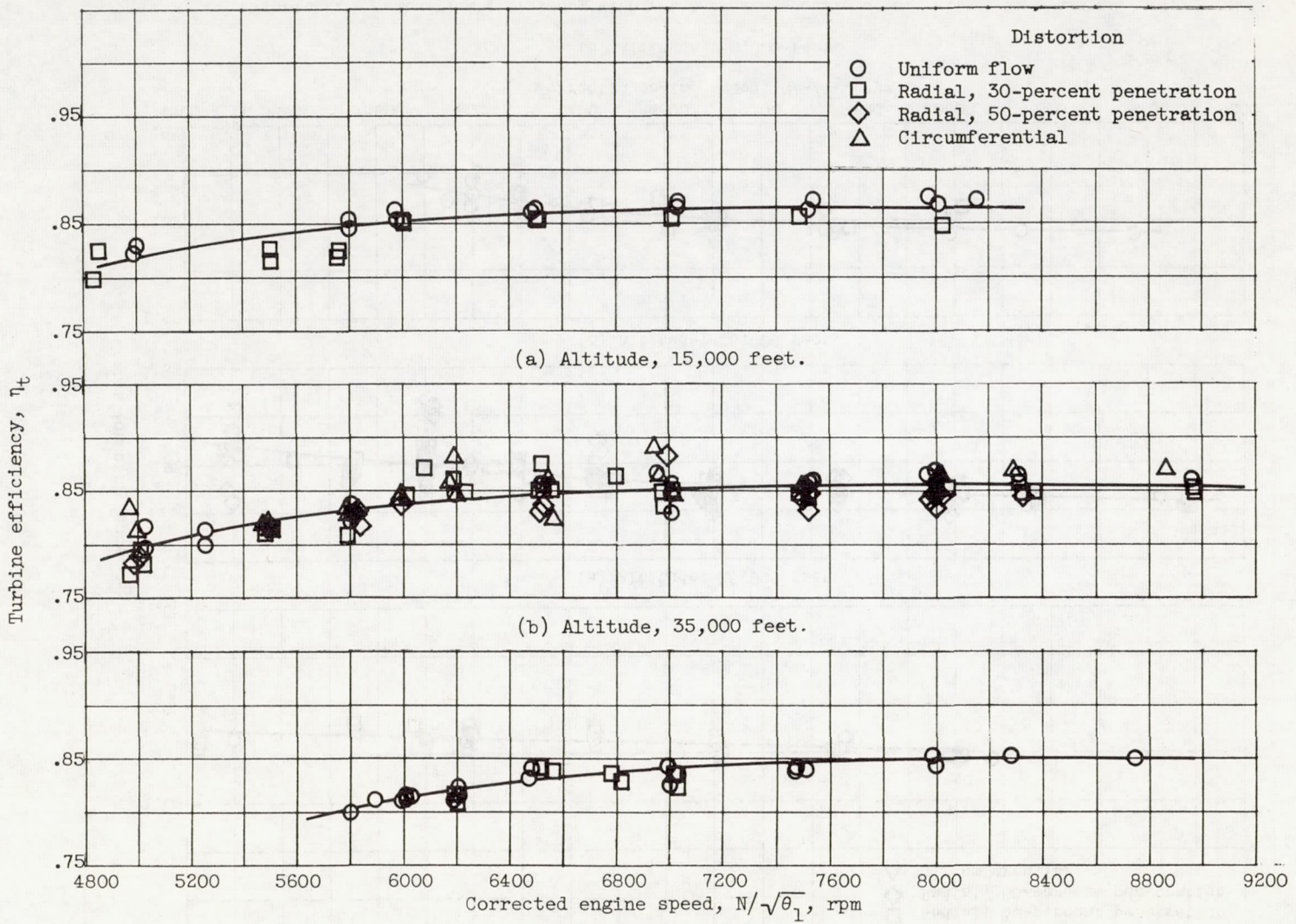

(a) Altitude, 15,000 feet.

(b) Altitude, 35,000 feet.

(c) Altitude, 50,000 feet.

Figure 12. - Turbine efficiency with rated exhaust-nozzle area. Flight Mach number, 0.8.

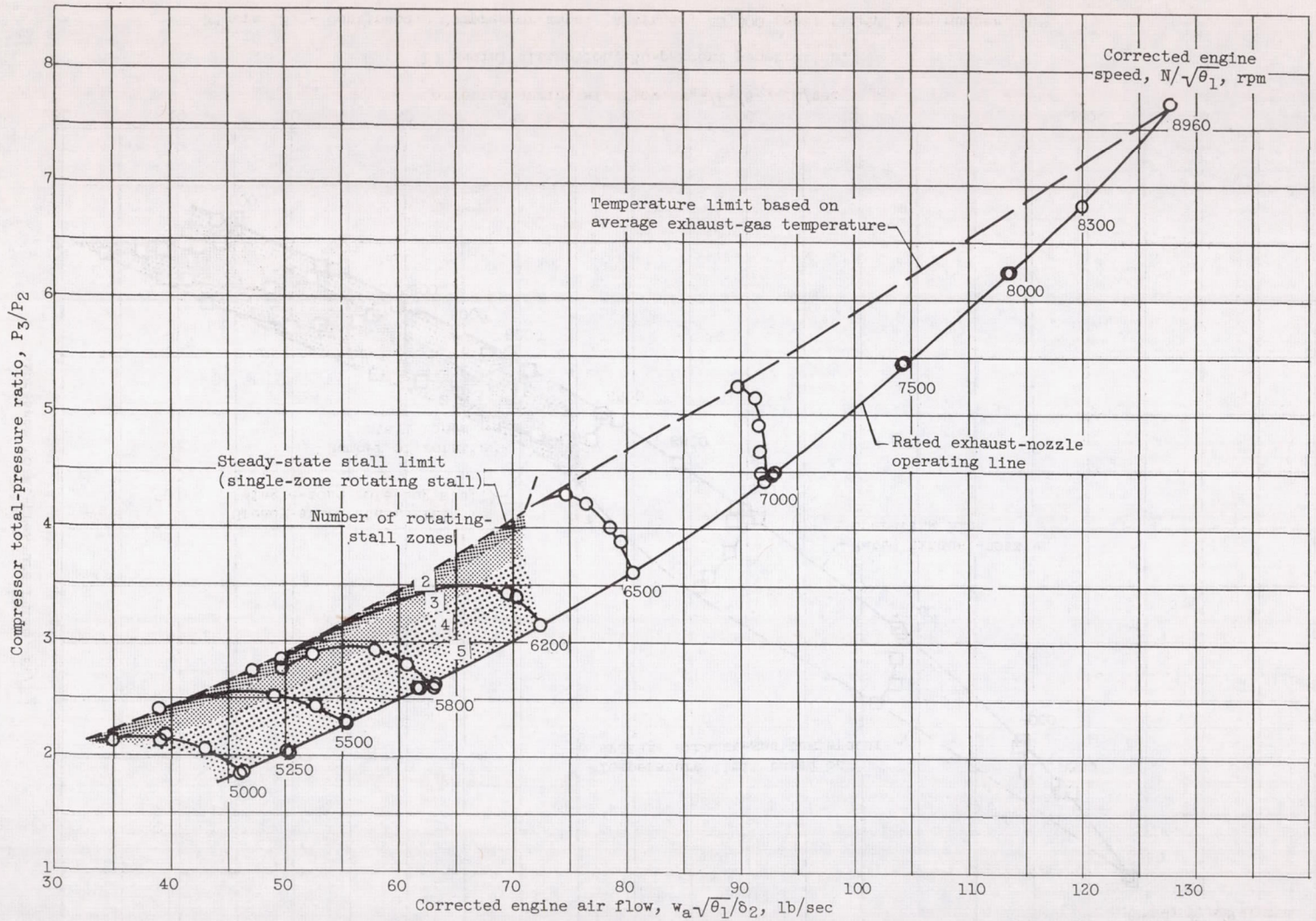

(a) Uniform flow.

Figure 13. - Compressor maps. Altitude, 35,000 feet; flight Mach number, 0.8.

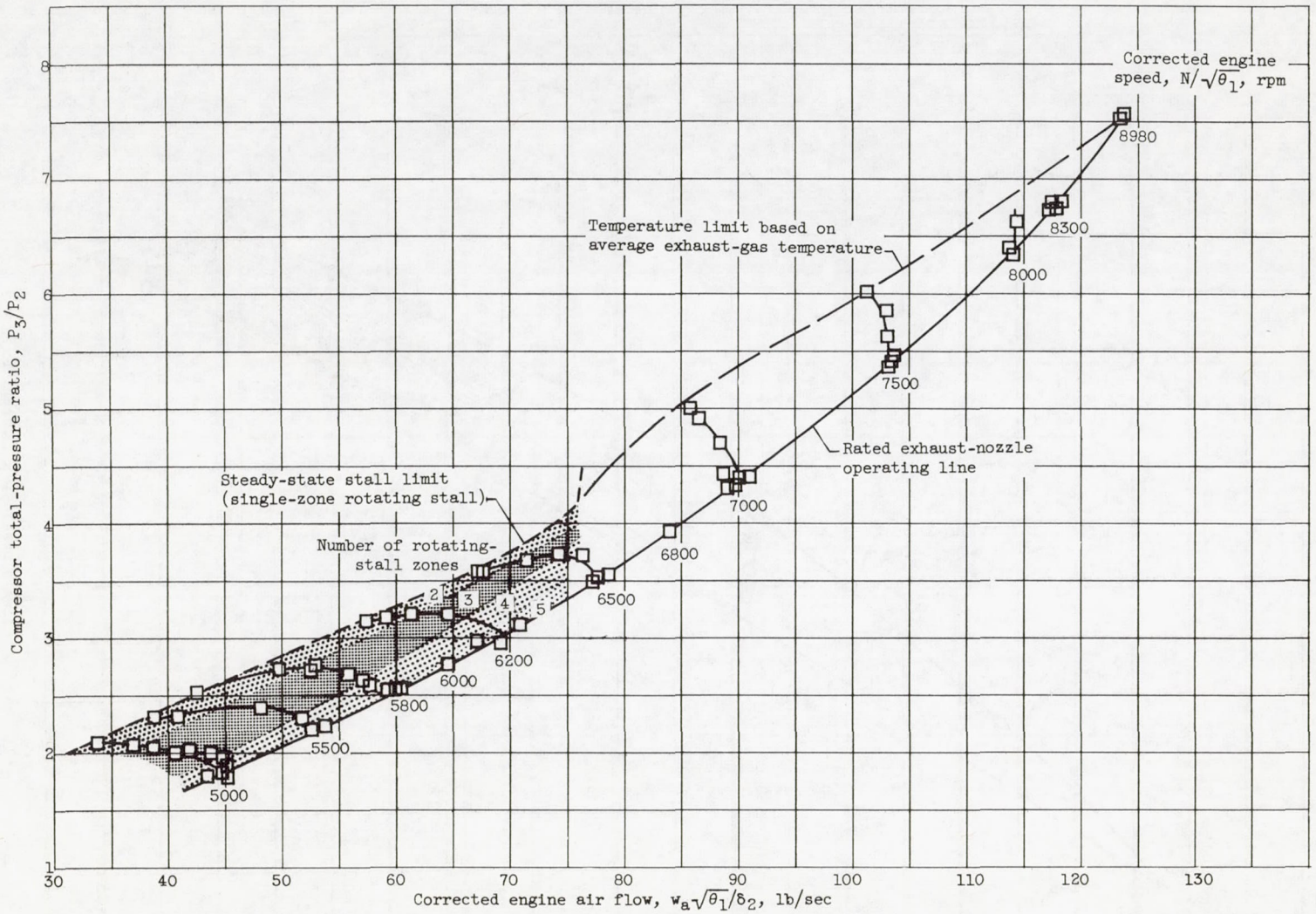

(b) Radial distortion, 30-percent penetration.

Figure 13. - Continued. Compressor maps. Altitude, 35,000 feet; flight Mach number, 0.8.

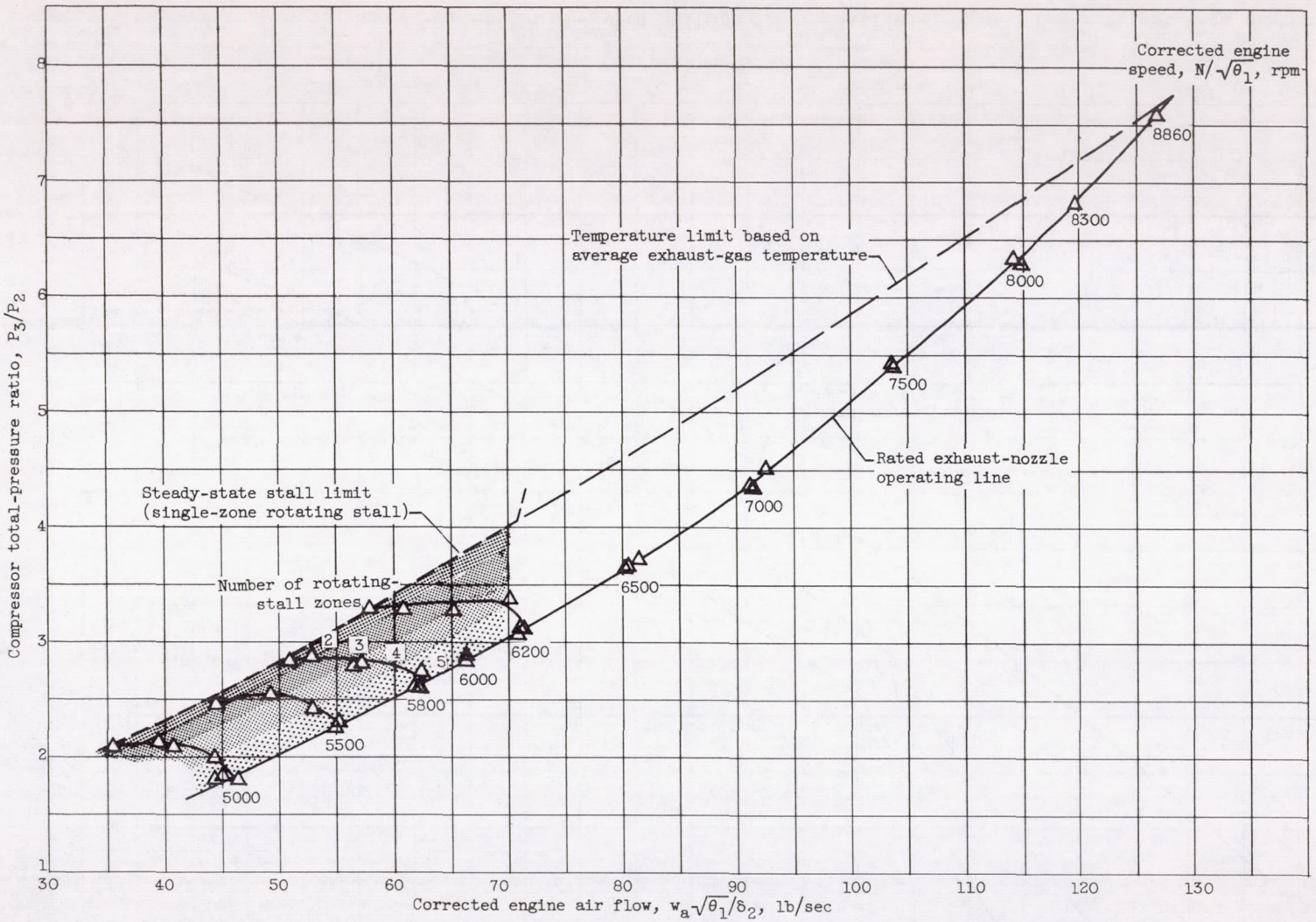

(c) Circumferential distortion.

Figure 13. - Concluded. Compressor maps. Altitude, 35,000 feet; flight Mach number, 0.8.

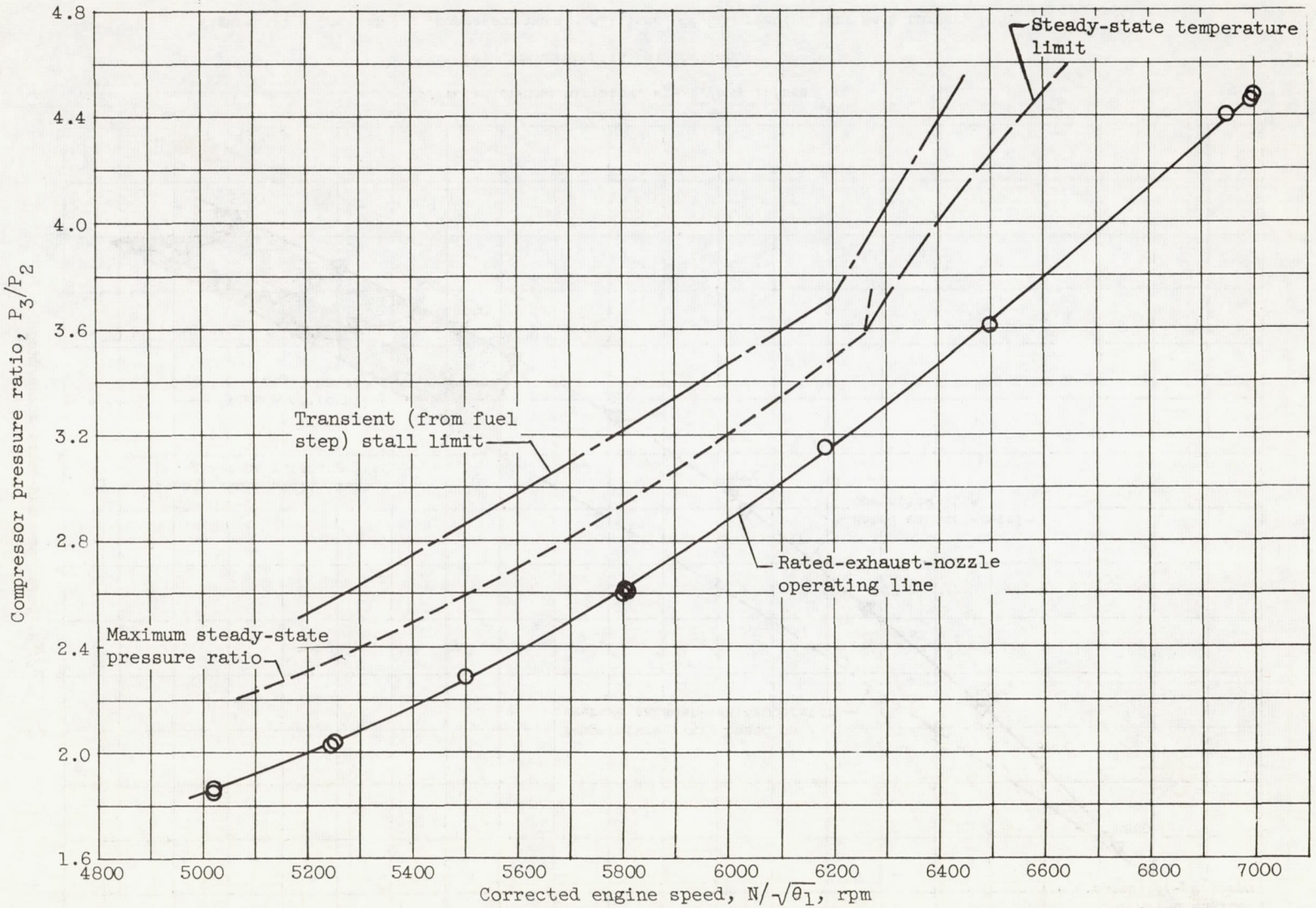

Figure 14. - Steady-state and transient limits with uniform flow. Altitude, 35,000 feet; flight Mach number, 0.8.

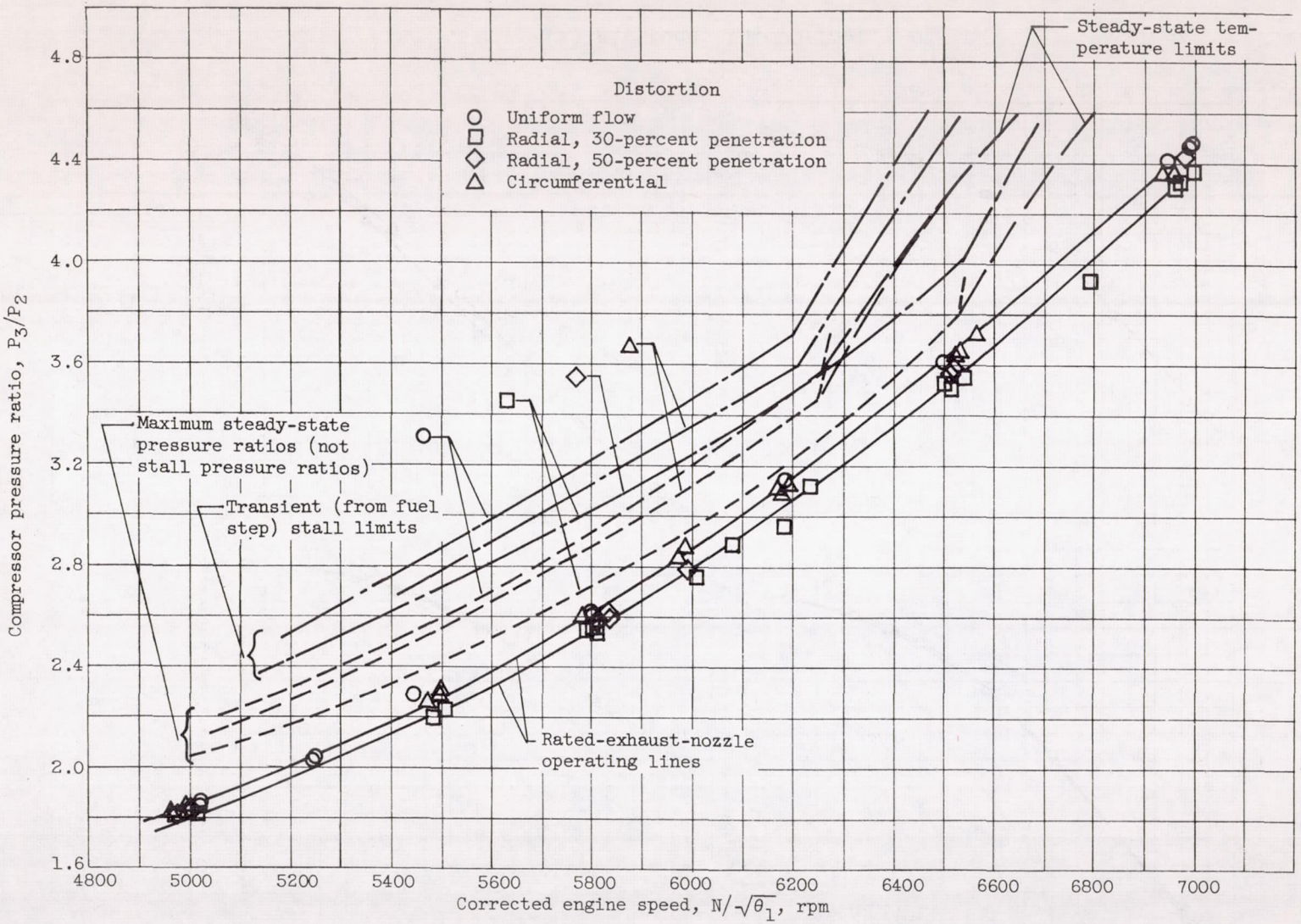

Figure 15. - Steady-state and transient limits. Altitude, 35,000 feet; flight Mach number, 0.8.

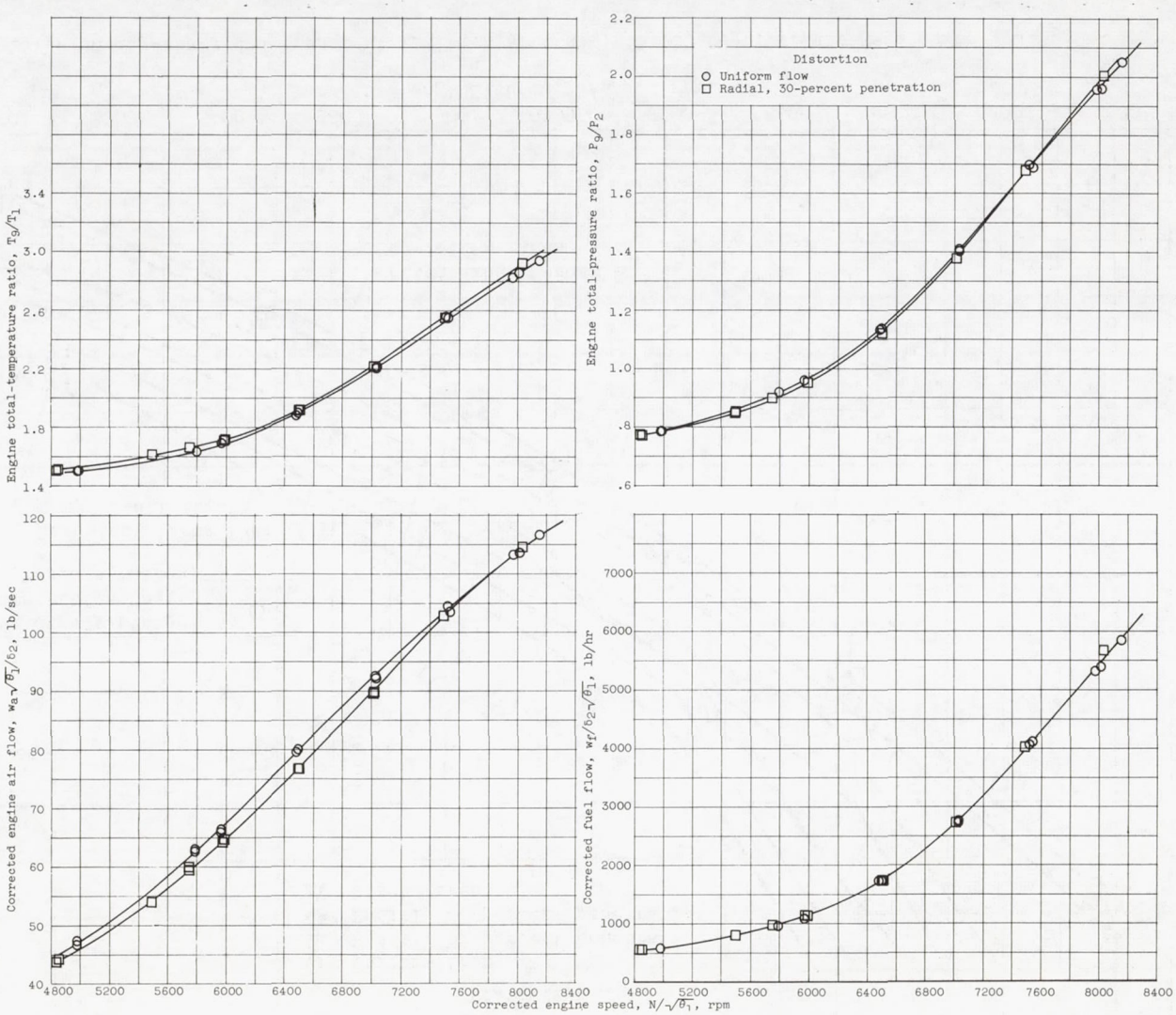

(a) Altitude, 15,000 feet.

Figure 16. - Engine pumping characteristics. Flight Mach number, 0.8.

(b) Altitude, 35,000 feet.

Figure 16. - Continued. Engine pumping characteristics. Flight Mach number, 0.8.

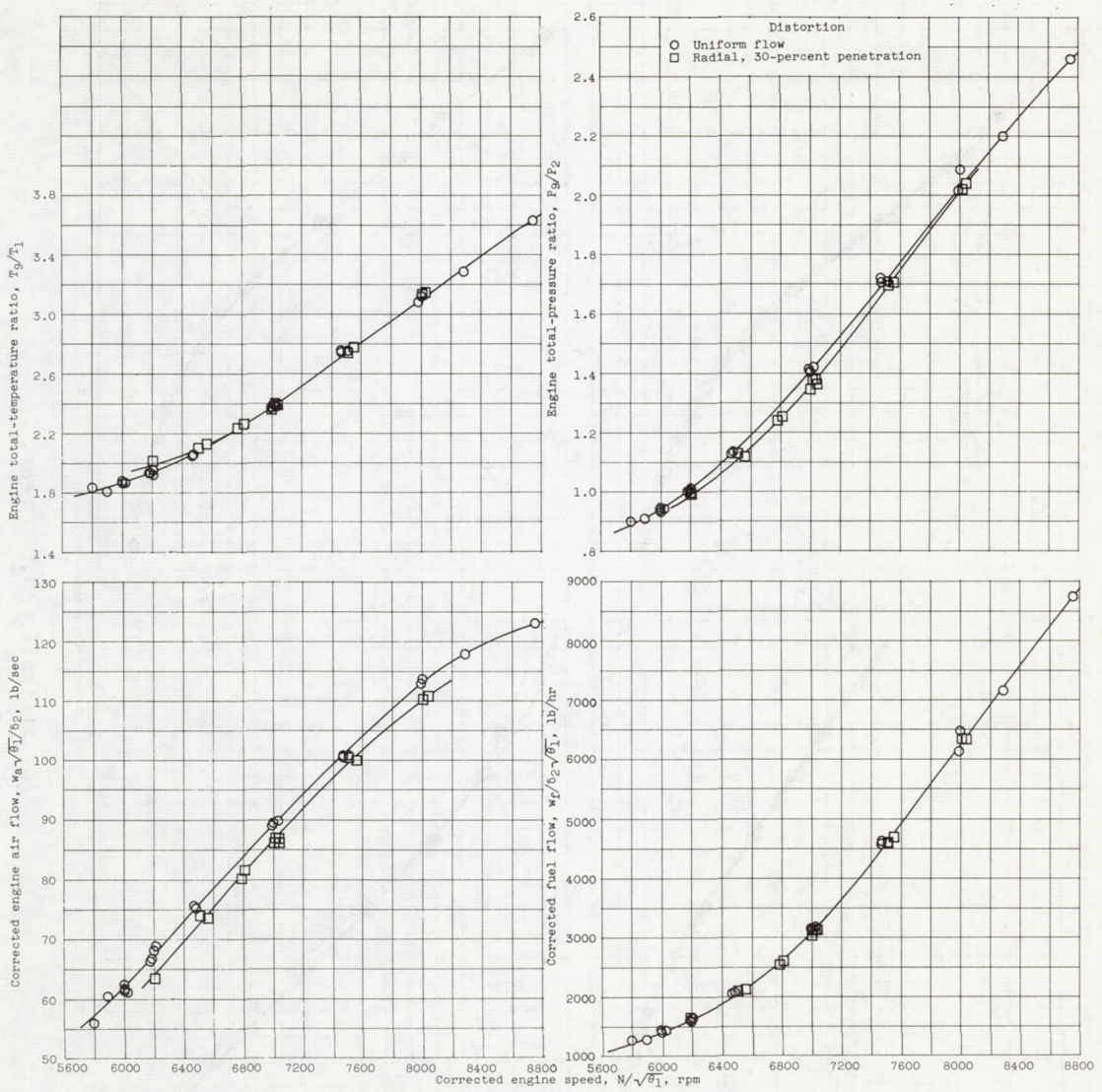

(c) Altitude, 50,000 feet.

Figure 16. - Concluded. Engine pumping characteristics. Flight Mach number, 0.8.

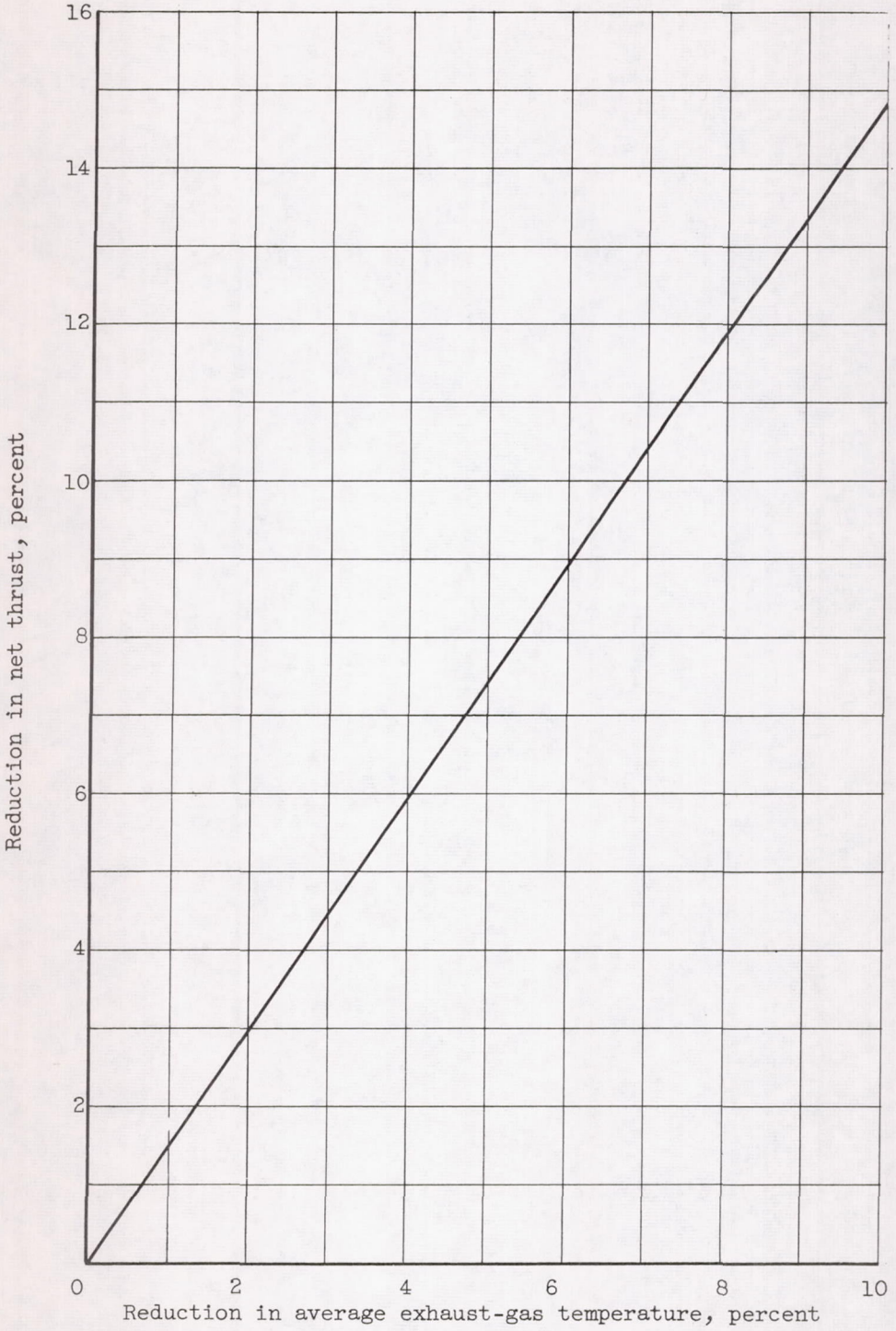

Figure 17. - Loss in net thrust due to reducing the average exhaust-gas temperature below rated with a fixed-area exhaust nozzle. Altitude, 35,000 feet; flight Mach number, 0.8.